Bulletin of the Seismological Society of America, Vol. 98, No. 2, pp. 593–606, April 2008, doi: 10.1785/0120070096

GPS Seismology: Application to the 2002 M_w 7.9 Denali Fault Earthquake

by Andria Bilich, John F. Cassidy, and Kristine M. Larson

Abstract The 2002 Denali fault, Alaska, earthquake (M_w 7.9) caused one or more components of most broadband seismometers in western Canada to clip, yet did not trigger strong-motion instruments, thus leaving a substantial gap in the seismic record of this event. However, the large-amplitude surface waves generated by this event were well recorded by the Global Positioning System (GPS) in the same region, out to epicentral distances of more than 3000 km. In this article, we explore the capabilities of GPS seismology, specifically how the relative strengths of GPS and seismic data sets can be exploited in order to more effectively study earthquake source characteristics and wave-propagation effects. High-rate (1-Hz) GPS data from 23 stations throughout western North America have been analyzed to derive displacement waveforms for this event, and the impact of instrumentation (GPS receiver model) and error-reduction strategy (modified sidereal and spatial filtering) on the noise characteristics of displacement time series at each GPS site was assessed. After applying error-reduction methods to GPS displacements, the final average noise floors of 0.5 cm in the horizontal and 1.5 cm in the vertical indicate that large dynamic displacements are observable by GPS. We validate the GPS displacements by comparing broadband seismic recordings (integrated to displacement) with GPS recordings for four effectively colocated sets of instruments. We show excellent agreement between the unclipped seismic and GPS recordings of the surface waves from the Denali earthquake over the period range of 10–50 sec and for ground displacements exceeding about 1.0 cm. Thus, a large GPS displacement data set is now available for western North America, an area where records of this event were previously missing or incomplete. The final GPS seismograms are archived at Incorporated Research Institutions for Seismology (IRIS) for public use in future studies of the 2002 Denali earthquake.

Introduction

The Global Positioning System (GPS) is a powerful tool for Earth studies, capable of representing displacements occurring over a range of temporal and spatial scales. Historically, permanent GPS stations have been operated at 30 sec or lower sample rates, and the GPS data were analyzed to yield one position solution per day. These data rates and methods are geared toward studying long-period Earth deformations such as plate tectonics or postglacial rebound (Segall and Davis, 1997) and are insufficient for monitoring short-period and/or short-duration motions such as waves generated by earthquakes.

Recent advances in receiver technology and increased data storage capabilities have raised interest in retasking GPS as a seismometer for large-magnitude events. An instrument capable of measuring seismic wave fields must be able to sample and record displacements at a rate of a few seconds to subsecond sample intervals. Receiver technology now enables sampling and permanent recording of GPS data at these high rates (e.g., 1 sample/sec or 1 Hz) and sometimes higher rates. Using 1-Hz GPS range data and solving for position at every data epoch, the resulting displacement time series are capable of representing seismic wave fields for large-magnitude events. Recent events successfully observed with high-rate GPS networks include the 2002 Denali (Kouba, 2003; Larson *et al.*, 2003; Bock *et al.*, 2004), 2003 Tokachi-Oki (Miyazaki *et al.*, 2004; Emore *et al.*, 2007), 2003 San Simeon (Ji *et al.*, 2004; Wang *et al.*, 2007), and 2004 Sumatra-Andaman (Ohta *et al.*, 2006) events. Using GPS receivers to monitor higher frequencies (>1 Hz) is possible if the receiver is set to sample at that rate, but ultimately the tracking bandwidth of the receiver will limit the amplitudes of the very highest frequency signals.

The differences between seismometers and GPS receivers are substantial and worth noting. The inertial seismometer, an electromechanical system, is originally at rest and when perturbed by ground motions produces a measur-

able signal (Aki and Richards, 1980). With digital seismometry, this signal is a series of point measurements of accelerations or velocities experienced directly by the instrument. By contrast, GPS receivers record range measurements to the GPS satellites, and the position of the GPS antenna at any moment must be estimated from these ranges (Parkinson *et al.*, 1996). GPS positions or displacements are computed in a terrestrial reference frame (Altamimi *et al.*, 2002), whereas seismographs produce direct measurements in an inertial reference frame. Seismometers are very sensitive and are capable of measuring moderate to large ($M > 5$) distant earthquakes, whereas the noise floor of high-rate GPS measurements limits GPS sensitivity to large-magnitude or nearby events (Ge *et al.*, 2000; Bock *et al.*, 2004; Bilich, 2006; Elósegui *et al.*, 2006).

Despite the differences, there exist benefits to GPS seismology that complement traditional seismic measurements. When recovery of displacements is desired, GPS directly estimates them, but seismic data must be integrated (once for velocity and twice for acceleration records) in order to recover displacement. Integration is an often error-prone process (Boore *et al.*, 2002) and has the potential to amplify noise and distort the true signal. In addition, seismic instruments can saturate or clip with sufficiently large ground motions so that the instrument does not record the full amplitude of local velocity or acceleration. GPS observations will not saturate in amplitude because, unlike seismometers, no instrument response limits the observation capability of the receiver. Seismometers operate in the presence of gravity, and tilt of the instrument can produce artificial horizontal acceleration, but GPS instruments are not affected in this way. Finally, seismic and GPS networks do not always coincide; there may be GPS data available in an area of interest but no seismometers, or vice versa. When earthquakes cause seismic instrumentation to clip or when seismometers are simply unavailable in an area, high-rate GPS observations may serve as a complementary data source.

2002 Denali Earthquake

The Denali Fault earthquake of 2002 provides an ideal case for the application of high-rate GPS. This earthquake occurred on 3 November 2002 at 22:12:41 coordinated universal time (UTC) and ruptured a total distance of 340 km (Eberhart-Phillips *et al.*, 2003). This large-magnitude (M_w 7.9) and shallow (5.0-km) earthquake began with reverse slip but quickly changed to right-lateral strike-slip motion as the rupture propagated to the east (Ozacar *et al.*, 2003). The combination of large size, strike-slip mechanism, upper-crustal depth, and long rupture zone resulted in strong directivity to the southeast (Velasco *et al.*, 2004). Seismic energy was focused along the great-circle path aligned with the rupture plane and led to triggered seismicity (Gomberg *et al.*, 2004) and amplified Love and Rayleigh waves (Velasco *et al.*, 2004) to the southeast.

These amplified surface waves, directed through western Canada and into the northwestern United States, were sufficiently large to send broadband seismometers offscale out to epicentral distances of 2200 km or more. Cassidy and Rogers (2004) reported that seismic instrumentation throughout western Canada clipped, and no strong-motion instruments were triggered. Figure 1 shows the distribution of the Canadian National Seismograph Network (CNSN) broadband stations operating at the time of this event. The Denali event saturated one or both of the horizontal components for 18 of the 22 broadband seismometers (Cassidy and Rogers, 2004), leaving few onscale seismic records in western Canada for this event.

High-rate (1-Hz) GPS successfully observed large-amplitude surface waves from this event in the region where broadband seismometers clipped or were unavailable (e.g., Kouba, 2003; Larson *et al.*, 2003), and surface waves remained observable by GPS as far away as southern California (Bock *et al.*, 2004). This study presents seismograms from a network of high-rate GPS stations (Fig. 1; Table 1) distributed throughout northwestern North America; the current network of 23 stations is expanded from the 8 stations discussed in Larson *et al.* (2003) and 11 stations of Kouba (2003) and utilizes some stations from Bock *et al.* (2004) for error-reduction purposes. Unlike the GPS displacement time series shown in some of these earlier works, the results presented here have been extensively filtered to reduce systematic errors in the displacement time series. These analysis and error-reduction methods and the noise characteristics of GPS displacements are described in the following section.

GPS Data and Analysis

Initial GPS displacement time series are estimated using a GPS-inferred positioning system (GIPSY; Lichten and Border, 1987). This research employs a network-positioning strategy in which station positions are defined in the international terrestrial reference frame, year 2000 realization (ITRF2000; Altamimi *et al.*, 2002). International GNSS (Global Navigation Satellite System) Service (IGS) precise orbits (Beutler *et al.*, 1999), also defined in ITRF2000, define the coordinates of the GPS satellites and are held fixed. Station positions are estimated as a white noise process at the data sampling rate of 1 sec (i.e., positions are computed at every epoch). The zenith tropospheric delay is estimated as a random walk process with a constraint of 9 mm^2 variance per hour. GPS observations below 15° elevation are excluded to minimize errors from multipath. The position of station GODE, located far from the region of observable ground motions, is constrained with an *a priori* sigma of 1.0 cm and is not estimated stochastically. This constraint is added to minimize rotation of the GPS network. GIPSY estimates clocks explicitly relative to a reference clock, and in this study station AMC2 serves as a reference clock. This clock estimation strategy is nearly equivalent to double differencing of clocks used by other software. Additional information on analysis

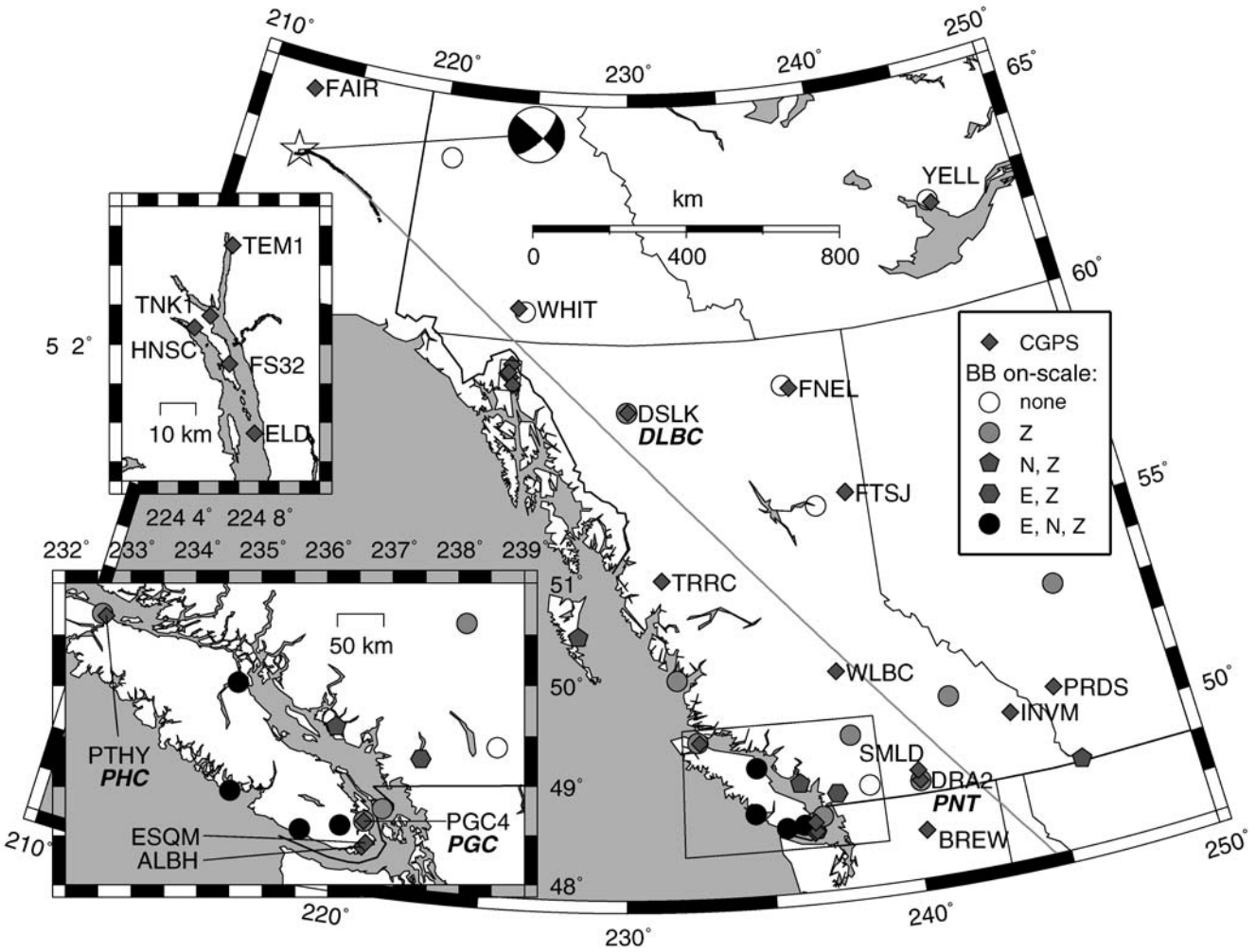

Figure 1. Map of CNSN broadband (BB) seismometers (circles, octagons, and pentagons) and continuously operating GPS stations (CGPS, diamonds) operating at the time of the Denali event; for the seismometers, the symbol shape and shading indicate which seismometer components remained onscale during the Denali fault earthquake (Cassidy and Rogers, 2004). Station labels apply only to stations examined in this study: GPS stations (normal text) and collocated seismometers with onscale verticals (bold oblique text). Some characteristics of the 2002 Denali fault earthquake are also given: epicenter, star; surface rupture, heavy black line; earthquake focal mechanism (Global CMT) and line of preferential directivity, light straight line. Inset map locations are marked by light boxes.

strategy can be found in Larson *et al.* (2003), Miyazaki *et al.* (2004), and Bilich (2006).

The large number of receiver models and firmware versions (Table 1) present in this network provide an interesting opportunity to assess noise differences in computed high-rate positions. The noise in GPS positions is characterized by computing the power spectral density (PSD) of each station's time series for the 1600 sec immediately before the Denali fault event began, when no actual displacements occur. Visual inspection of the PSD for each station and component shows that high-rate GPS displacements are approximately white at high frequencies and demonstrate power-law dependence at lower frequencies (Fig. 2). To quantify noise characteristics, we assume each spectrum is white noise over 0.1–0.5 Hz (2–10-sec periods) and demonstrates uniform power-law noise behavior over 0.01–0.1 Hz (10–100-sec periods), then compute the white noise amplitude σ_{WH} and spectral index n for these respective PSD sections. The white noise amplitude is a function of each power spectrum integrated over the white noise frequencies

$$\sigma_{WH}^2 = \int_{0.1\text{ Hz}}^{0.5\text{ Hz}} P(f)\, df. \tag{1}$$

The specific type of power law noise for each spectrum is characterized by the spectral index n (Agnew, 1992). Power law noise is described in the frequency domain by

$$P(f) = P_0/f^n, \tag{2}$$

and we compute n by finding the slope of the best-fit straight line to the PSD in log–log space. Summaries of white noise amplitude and spectral index for each station and component are provided in Tables 2 and 3.

Table 1

GPS Station Position, Network, and Equipment Information

Site	Latitude (deg)	Latitude (deg)	Height (m)	Network	Receiver Mode and Firmware	Antenna Model and Radome	Purpose
ALBH	48.3898	236.5125	31.7	CACS/WCDA/IGS	AOA BENCHMARK ACT 3.3.32.2N	AOAD/M_T EMRA	P
BREW	48.1315	240.3174	238.6	IGS	ASHTECH UZ-12 CJ10	ASH701945C_M SCIT	P
DRA2	49.3226	240.3750	542.2	CACS/WCDA/IGS	AOA BENCHMARK ACT 3.3.32.3	AOAD/M_T	P
DSLK	58.4358	230.0110	818.3	CSRS	TRIMBLE 4000SSI 7.29/3.03/Boot3.33	TRM22020.00 + GP	P
ELDD	58.9720	224.7777	10.2	AeroMap	TRIMBLE 5700 NP 1.22/SP 0.00	TRM41249.00	P
ESQM	48.4293	236.5713	21.1	CSRS	TRIMBLE 4700 1.30/Boot1.00	TRM33429.20 + GP	P
FAIR	64.9780	212.5008	319.8	IGS	ASHTECH UZ-12 CJ00	AOAD/M_T JPLA	P
FNEL	58.8053	237.2679	439.8	CSRS	TRIMBLE 4000SSI 7.29/3.03/Boot3.33	TRM22020.00 + GP	P
FS32	59.1487	224.6530	8.2	AeroMap	TRIMBLE 5700 NP 1.22/SP 0.00	TRM41249.00	P
FTSJ	56.2550	239.1514	708.5	CSRS	TRIMBLE 4000SSI 7.29/3.03/Boot3.33	TRM22020.00 + GP	P
HNSC	59.2423	224.4822	10.5	AeroMap	TRIMBLE 4000SSI 7.29/3.07	TRM22020.00 − GP	P
INVM	50.5092	243.9714	828.2	CSRS	TRIMBLE 4000SSI 7.29/3.07/Boot3.33	TRM22020.00 + GP	P
MSOL	46.9294	245.8911	958.5	CORS	TRIMBLE 4000SSI 7.32	TRM33429.00 + GP	P
PGC4	48.6485	236.5490	3.6	WCDA	TRIMBLE 4700 1.30/Boot1.00	TRM33429.20 + GP	P
PRDS	50.8713	245.7065	1248.5	CACS/IGS	AOA SNR-12 ACT 3.3.32.2N	AOAD/M_T	P
PTHY	50.6856	232.6247	1.6	CSRS	TRIMBLE 4000SSI 7.29/3.07/Boot3.33	TRM14532.00GP	P
SMLD	49.5655	240.3558	431.9	CSRS	TRIMBLE 4000SSI 7.29/3.07/Boot3.34	TRM22020.00 + GP	P
TEM1	59.4502	224.6698	14.3	AeroMap	TRIMBLE 4000SSI 7.29/3.07	TRM22020.00 − GP	P
TNK1	59.2722	224.5595	12.5	AeroMap	TRIMBLE 4000SSI 7.29/3.07	TRM22020.00 − GP	P
TRRC	54.5148	231.3734	60.4	CSRS	TRIMBLE 4000SSI 7.29/3.07/Boot3.33	TRM22020.00 + GP	P
WLBC	52.1305	237.8632	607.7	CSRS	TRIMBLE 4000SSI 7.29/3.07/Boot3.34	TRM29659.00	P
WHIT	60.7505	224.7779	1427.4	CACS/WCDA/CSRS	AOA SNR-8000 ACT TURBO 3.3.32.2N	AOAD/M_T	P
YELL	62.4809	245.5193	181.0	CSRS	AOA BENCHMARK ACT TURBO 3.3.32.2N	AOAD/M_T	P
AMC2	38.8031	255.4754	1912.4	IGS	ASHTECH Z-12 IL01-1D04-MCF-12MX	AOAD/M_T	R
GODE	39.0216	283.1731	14.2	IGS	AOA SNR-8000 ACT 3.3.32.5	AOAD/M_T JPLM	R
FVPK	33.6623	242.0643	−11.5	SCIGN	ASHTECH Z-12	ASH701933B_M SCIT	S
OEOC	33.7658	242.2599	358.6	SCIGN	ASHTECH Z-12	ASH701945B_M SCIT	S
WHYT	33.6744	242.3565	265.4	SCIGN	ASHTECH Z-12	ASH701945B_M SCIT	S

Twenty-three stations for positioning, 2 reference stations, and 3 spatial filter stations. The network and purpose codes listed in the table are as follows.

Network Codes: AeroMap U.S., AeroMap (www.aeromap.com [last accessed October 2007]); Geological Survey of Canada, Canadian Active Control System, CACS; U.S. National Geodetic Survey, Continuously Operating Reference Stations, CORS; Geological Survey of Canada, Canadian Spatial Reference System, CSRS; International GNSS Service, IGS; Southern California Integrated GPS Network, SCIGN; and Geological Survey of Canada, Western Canada Deformation Array, WCDA.

Purpose Codes: high-rate positioning, P; reference station (clock or position), R; and spatial filtering station, S.

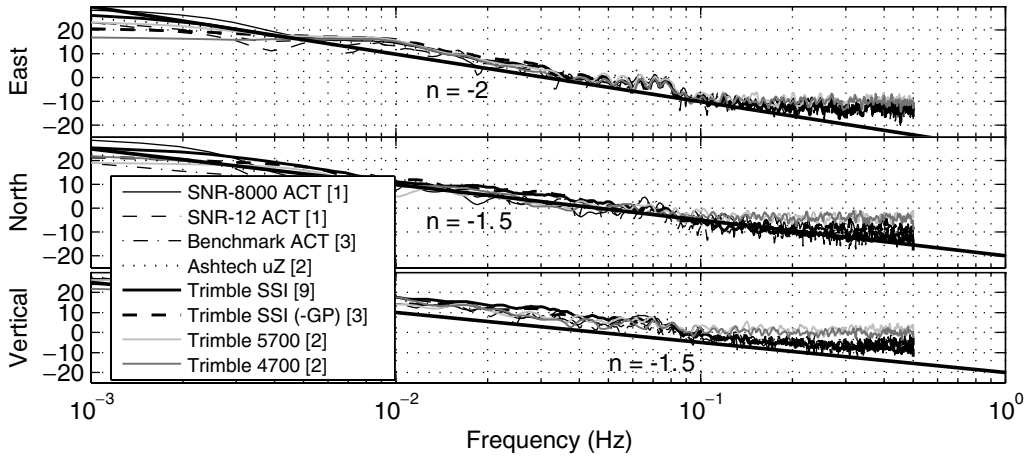

Figure 2. Average power spectral density of computed GPS positions for the 1600 sec before the Denali event began, expressed in dB of cm^2/Hz. Each average PSD profile is the mean of all stations using a particular receiver (number of stations contributing to each curve given in brackets in the legend); each station's PSD is the mean of separate PSDs for eight data segments with 50% overlap between adjacent segments. The heavy lines indicate the approximate spectral index n for each component (Table 3).

Many of the stations, receiver types, and position components possess comparable white noise amplitudes and spectral indices when the GPS data are first analyzed (Fig. 2). On average, the white noise amplitudes are $\sigma_{WH} = 0.05$–0.2 cm (Table 2) for our entire 23-station GPS network. Averaging over all stations, the east component has the lowest white noise amplitude (0.06 cm), followed by the north (0.09 cm), and vertical (0.15 cm), as expected, given better precision for horizontal over vertical components with GPS positioning and the distribution of satellites over North America at the time of the Denali event (Larson *et al.*, 2003). Looking at the 10–100-sec periods, the spectral index of -2 for the east indicates a random walk process, whereas the north and vertical components have generalized power law noise somewhere between flicker noise (-1) and random walk (Table 3).

If we break the stations into subgroups by receiver model, it becomes clear that some receivers have higher noise floors than others (Fig. 2). Specifically, the spectral power at high frequencies for Trimble 4700 and Trimble 5700 receivers is larger than all other models, by several dB for the north and vertical components, but only slightly larger for the east. This observation is mirrored by the average white noise amplitudes for north and vertical components: 0.14 and 0.23 cm for Trimble 4700/5700 as opposed to 0.07 and 0.12 cm for Trimble 4000SSI receivers and 0.09 and 0.15 cm for Ashtech micro-Z and ACT model receivers (Table 2). The east component of all three receiver groups has comparable white noise amplitudes, however. The spectral indices demonstrate no such breakout of receiver groups; the noise at 10–100-sec periods is dominated by processes such as multipath, which are independent of the receiver type.

Considering noise at frequencies described by the power law relationship, we note that GPS positions contain systematic apparent displacements of several centimeters (Fig. 3a), which are sometimes of equivalent magnitude to the desired signal, the seismic waves. Minimizing errors in the positions would make seismic phases more easily distinguishable from the GPS position noise and would yield a lower-noise seismogram. These errors or apparent displacements in GPS positions can be reduced through filtering methods, namely modified sidereal filtering (MSF) (Choi *et al.*, 2004) and spatial filtering, that recognize the daily repeatability or common-mode nature of positioning error sources; although these methods are becoming common in the geodesy literature, we review the principles of MSF and spatial filtering here for completeness.

Some systematic errors in the displacement time series appear to repeat on consecutive days for a given station (Fig. 3a), indicating that part of the error spectrum of high-rate GPS is nonrandom and is caused by repeatable errors such as multipath. These station-specific errors are minimized through MSF. This method draws upon the dependence of error repetition on satellite-receiver geometry (Genrich and Bock, 1992); position errors will repeat each day given identical relative positions of the satellite and receiving antenna. In MSF, a profile of position errors on one or more days is used to remove errors on the day of interest, resulting in a lower noise floor and less structured noise characteristics (Fig. 3b). In this study, data from 2 and 4 November 2002 are used to improve the time series from 3 November 2002. The error repeat time of 247 sec less than a solar day characterizes the majority of stations in this study (Bilich, 2006), and this value is used to construct and remove the MSF error profile for each station. While 247 sec is appropriate for western North America for the time period immediately following the Denali earthquake, in general, the repeat time of the position time series will vary as the satellites in view change. A more general technique is described

Table 2

Noise Characteristics of GPS Displacements

Site	Receiver Model	East						North						Vertical					
		s_0	s_{filt}	Δs	R_0	R_{filt}	ΔR	s_0	s_{filt}	Δs	R_0	R_{filt}	ΔR	s_0	s_{filt}	Δs	R_0	R_{filt}	ΔR
WHIT	SNR-8000 ACT	0.06	0.06	0.00	1.4	0.5	−0.9	0.09	0.09	0.00	1.5	0.5	−1.0	0.12	0.12	0.00	1.9	1.0	−0.9
PRDS	SNR-12 ACT	0.07	0.08	0.00	0.9	0.4	−0.5	0.09	0.09	0.00	1.1	0.4	−0.7	0.17	0.17	0.00	1.4	0.8	−0.6
ALBH	Benchmark ACT	0.05	0.03	−0.02	0.8	0.4	−0.4	0.08	0.07	0.00	0.7	0.4	−0.2	0.14	0.13	−0.01	1.3	0.8	−0.5
DRA2	Benchmark ACT	0.09	0.09	0.00	1.0	0.4	−0.6	0.11	0.12	0.00	1.2	0.4	−0.8	0.18	0.18	0.01	1.9	1.4	−0.5
YELL	Benchmark ACT	0.05	0.05	0.00	1.2	0.5	−0.7	0.08	0.08	0.00	0.6	0.5	0.0	0.17	0.17	−0.01	2.8	1.1	−1.7
BREW	Ashtech uZ	0.08	0.08	0.00	12.0	0.4	−0.6	0.09	0.09	0.00	1.3	0.5	−0.8	0.16	0.16	0.00	1.7	1.5	−0.2
FAIR	Ashtech uZ	0.07	0.07	0.00	1.3	0.5	−0.8	0.10	0.10	0.00	0.9	0.7	−0.1	0.14	0.14	0.00	1.9	1.4	−0.6
DSLK	Trimble 4000SSI	0.11	0.06	−0.05	2.9	0.8	−2.1	0.13	0.12	−0.01	2.5	1.2	−1.3	0.21	0.16	−0.06	7.4	2.4	−5.0
FNEL	Trimble 4000SSI	0.05	0.04	−0.02	1.5	0.4	−1.1	0.07	0.07	0.01	1.9	0.9	−1.0	0.12	0.12	0.01	3.3	1.9	−1.4
FTSJ	Trimble 4000SSI	0.05	0.03	−0.02	1.9	0.4	−1.5	0.06	0.06	0.00	1.9	0.9	−1.0	0.11	0.08	−0.03	2.2	1.4	−0.8
INVM	Trimble 4000SSI	0.04	0.03	−0.02	1.0	0.4	−0.6	0.06	0.06	0.00	1.1	0.6	−0.5	0.11	0.09	−0.02	2.8	1.0	−1.8
MSOL	Trimble 4000SSI	0.04	0.03	−0.02	0.9	0.3	−0.6	0.05	0.05	0.00	0.8	0.5	−0.3	0.09	0.07	−0.02	1.7	0.9	−0.8
PTHY	Trimble 4000SSI	0.05	0.02	−0.03	1.3	0.5	−0.9	0.05	0.05	0.00	0.7	0.6	−0.1	0.09	0.07	−0.02	2.2	1.0	−1.2
SMLD	Trimble 4000SSI	0.05	0.02	−0.02	0.9	0.4	−0.6	0.06	0.06	0.00	0.9	0.7	−0.2	0.11	0.09	−0.02	2.1	1.2	−0.9
TRRC	Trimble 4000SSI	0.05	0.03	−0.02	1.2	0.6	−0.5	0.06	0.07	0.00	1.5	0.9	−0.6	0.10	0.09	−0.02	2.8	1.0	−1.9
WLBC	Trimble 4000SSI	0.05	0.02	−0.03	1.3	0.5	−0.8	0.06	0.06	0.00	1.2	0.7	−0.5	0.11	0.09	−0.02	2.8	1.5	−1.3
HNSC	Trimble 4000SSI (−GP)	0.06	0.06	0.00	1.0	0.6	−0.4	0.09	0.08	−0.01	1.1	1.0	−0.1	0.12	0.12	−0.01	1.6	1.3	−0.3
TEM1	Trimble 4000SSI (−GP)	0.06	0.06	0.00	0.9	0.6	−0.3	0.09	0.08	−0.01	1.1	1.1	0.0	0.12	0.11	−0.01	1.8	1.7	−0.1
TNK1	Trimble 4000SSI (−GP)	0.06	0.06	0.00	0.9	0.5	−0.4	0.09	0.08	−0.01	0.9	1.0	0.1	0.12	0.11	−0.01	1.6	1.2	−0.3
ELDD	Trimble 5700	0.07	0.07	0.00	1.1	0.4	−0.6	0.14	0.14	0.00	0.8	0.8	0.0	0.25	0.25	0.00	1.6	1.8	0.2
FS32	Trimble 5700	0.07	0.07	0.00	1.0	0.5	−0.5	0.14	0.14	0.00	0.9	0.9	0.0	0.25	0.25	0.00	1.9	1.7	−0.2
ESQM	Trimble 4700	0.07	0.05	−0.01	0.8	0.3	−0.5	0.13	0.13	0.00	1.0	0.5	−0.5	0.20	0.20	0.00	1.6	0.8	−0.7
PGC4	Trimble 4700	0.07	0.05	−0.01	0.8	0.3	−0.5	0.13	0.13	0.00	0.9	0.6	−0.3	0.21	0.21	0.00	1.3	0.9	−0.3
Trimble 4700/5700 rx		0.07	0.06	−0.01	0.9	0.4	−0.5	0.14	0.14	0.00	0.9	0.7	−0.2	0.23	0.23	0.00	1.6	1.3	−0.3
Trimble 4000SSI rx		0.06	0.04	−0.02	1.3	0.5	−0.8	0.07	0.07	0.00	1.3	0.8	−0.5	0.12	0.10	−0.02	2.7	1.4	−1.3
Ashtech and ACT rx		0.07	0.07	0.00	1.1	0.4	−0.6	0.09	0.09	0.00	1.0	0.5	−0.5	0.15	0.15	0.00	1.8	1.1	−0.7
All stations		0.06	0.05	−0.01	1.2	0.5	−0.7	0.09	0.09	0.00	1.2	0.7	−0.4	0.15	0.14	−0.01	2.2	1.3	−0.9

Noise characteristics of all 23 GPS stations with estimated positions, before (subscript 0) and after (subscript filt) sidereal and spatial filtering, where s is a white noise amplitude obtained by integrating the power spectrum over 2–10-sec periods and R is the rms of the position time series, both in centimeters. The differences between raw and filtered values are given in the Δ columns. Stations HNSC, TEM1, TNK1, ELDD, and FS32 were not sidereally filtered, as these stations were operational only on the day of the earthquake; spatial filtering was still implemented.

Table 3
Spectral Indices of GPS Displacement Power Spectra

Site	Receiver Model	East			North			Vertical		
		n_0	n_{filt}	Δn	n_0	n_{filt}	Δn	n_0	n_{filt}	Δn
WHIT	SNR-8000 ACT	−1.9	−0.6	1.3	−1.0	−0.4	0.7	−1.1	0.1	1.3
PRDS	SNR-12 ACT	−1.9	−0.6	1.2	−1.7	−1.0	0.7	−1.7	−1.1	0.6
ALBH	Benchmark ACT	−2.2	−0.7	1.4	−1.5	−0.5	1.1	−1.7	−0.6	1.1
DRA2	Benchmark ACT	−1.8	−0.5	1.3	−2.2	−0.7	1.4	−2.1	−0.8	1.3
YELL	Benchmark ACT	−2.0	−0.5	1.5	−1.5	−0.8	0.6	−1.6	−0.8	0.8
BREW	Ashtech uZ	−2.0	−0.9	1.1	−1.7	−0.9	0.8	−1.7	−1.1	0.6
FAIR	Ashtech uZ	−1.7	0.1	1.8	−0.7	0.0	0.7	−0.6	0.3	0.9
DSLK	Trimble 4000SSI	−1.9	−1.8	0.1	−2.1	−1.6	0.5	−2.1	−1.9	0.1
FNEL	Trimble 4000SSI	−2.2	−1.9	0.3	−1.9	−1.5	0.4	−1.9	−1.8	0.0
FTSJ	Trimble 4000SSI	−2.3	−2.0	0.3	−2.0	−1.7	0.3	−1.6	−2.2	−0.5
INVM	Trimble 4000SSI	−2.3	−1.4	0.8	−1.7	−1.3	0.4	−1.9	−1.6	0.3
MSOL	Trimble 4000SSI	−2.3	−1.3	1.1	−1.7	−1.4	0.3	−1.8	−1.7	0.2
PTHY	Trimble 4000SSI	−2.1	−1.3	0.8	−1.6	−1.4	0.2	−1.6	−1.4	0.3
SMLD	Trimble 4000SSI	−2.1	−1.2	0.8	−1.7	−1.8	−0.1	−2.1	−1.9	0.3
TRRC	Trimble 4000SSI	−2.1	−1.3	0.8	−1.6	−1.5	0.1	−1.7	−1.8	−0.1
WLBC	Trimble 4000SSI	−2.3	−1.5	0.8	−1.7	−1.2	0.5	−1.9	−1.8	0.2
HNSC	Trimble 4000SSI (−GP)	−2.0	−1.4	0.6	−1.9	−1.7	0.1	−1.8	−1.9	−0.1
TEM1	Trimble 4000SSI (−GP)	−2.2	−1.4	0.7	−1.8	−1.9	−0.1	−1.7	−2.0	−0.3
TNK1	Trimble 4000SSI (−GP)	−2.4	−1.8	0.6	−1.5	−1.7	−0.2	−2.0	−2.1	−0.1
ELDD	Trimble 5700	−2.0	−0.9	1.1	−0.9	−0.8	0.1	−1.1	−1.2	−0.2
FS32	Trimble 5700	−1.9	−1.3	0.6	−1.2	−1.2	0.0	−1.5	−1.5	0.0
ESQM	Trimble 4700	−2.1	−0.5	1.7	−1.3	0.1	1.4	−1.4	−0.2	1.3
PGC4	Trimble 4700	−2.1	−0.1	2.0	−1.4	−0.5	0.9	−1.4	−0.5	0.9
Trimble 4700/5700 rx		−2.0	−0.7	1.4	−1.2	−0.6	0.6	−1.4	−0.9	0.5
Trimble 4000SSI rx		−2.2	−1.5	0.6	−1.8	−1.6	0.2	−1.8	−1.8	0.0
Ashtech and ACT rx		−1.9	−0.5	1.4	−1.5	−0.6	0.9	−1.5	−0.6	0.9
All stations		−2.1	−1.1	1.0	−1.6	−1.1	0.5	−1.7	−1.3	0.4

Spectral indices n derived from power spectral curves for all 23 GPS stations with estimated positions; see Table 2 for a description of subscripts and sidereal filtering of station data.

by Larson *et al.* (2007), in which the repeat period is allowed to vary throughout the day and by station.

After MSF, some nonwhite errors remain, which are common to simultaneous records at distant GPS stations (Fig. 4a). These systematic errors are due to unmodeled errors at the reference site and/or any unmodeled error affecting all stations simultaneously, and are addressed through spatial filtering or stacking (Wdowinski *et al.*, 1997; Larson *et al.*, 2007). In spatial filtering, positions from several stations outside the region of active deformation are combined to form a profile of the common-mode error. When this profile is subtracted from the station of interest, noise is further reduced (Fig. 4b). For the majority of results in this study, three sites in southern California at approximately 33° N (Table 1) are used for spatial filtering. For stations north of approximately 60° N, the spatial filter is instead constructed from stations in the network (i.e., ALBH, DRA2, and BREW) at 48–49° N. Because of their higher latitudes, these stations have a GPS-satellite distribution that is more similar to northern Canada and better represents the common-mode error at $>60°$ N (Bilich, 2006).

MSF and spatial filtering primarily address errors at >10-sec periods, with varying degrees of power reduction in the different components. Figure 5 presents examples of the raw positions and filters applied to these positions for station ALBH, as observed in the ~1600 sec before the Denali event began. By comparing the PSD of the raw positions to the spectra of the MSF and spatial filters (Fig. 5), it is apparent that MSF captures variability in the 80–1000-sec range, where the largest amplitude oscillations occur, whereas the spatial filter or stack removes some residual power of smaller amplitude at 10–80-sec periods. The net effect of MSF and spatial filtering is to whiten the spectra of the positions while substantially reducing the root mean square (rms) of the time series, in this case to 0.4 cm for the horizontal components and 0.8 cm for the vertical. Spectral power reduction at periods >10 sec also leads to changes in the characteristic spectral index n (Table 3). Taking all stations and receiver types as a whole, the noise in all components is reduced to approximately flicker noise ($n = -1$), consistent with the analysis of filtered instantaneous positioning results in Bock *et al.* (2004). Analyzing the stations by receiver model, we note that the Trimble 4000SSI receivers have a smaller n reduction (change of 0.6, 0.2, and 0.0 for east, north, and vertical components, respectively) than their Trimble 4700/5700 (1.4, 0.6, 0.5) and Ashtech/ACT (1.4, 0.9, 0.9) counterparts. Trimble 4000SSI stations in this network benefit most from MSF and spatial

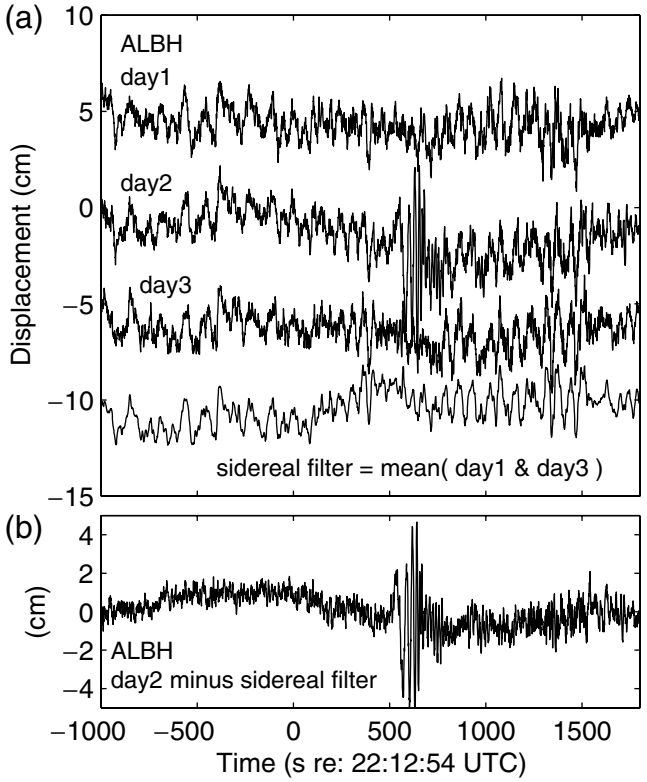

Figure 3. Modified sidereal filtering (MSF) of the east component at station ALBH. (a) To build the MSF, raw positions for the day before (day 1) and day after (day 3) are time shifted by the orbital repeat period (23 hr, 55 min, 53 sec), then pointwise averaged and smoothed with a seven-point sliding boxcar to form the filter profile. (b) To apply the modified sidereal filter, the filter profile is subtracted from positions on the day of the earthquake (day 2), resulting in a filtered time series that clearly displays the surface waves.

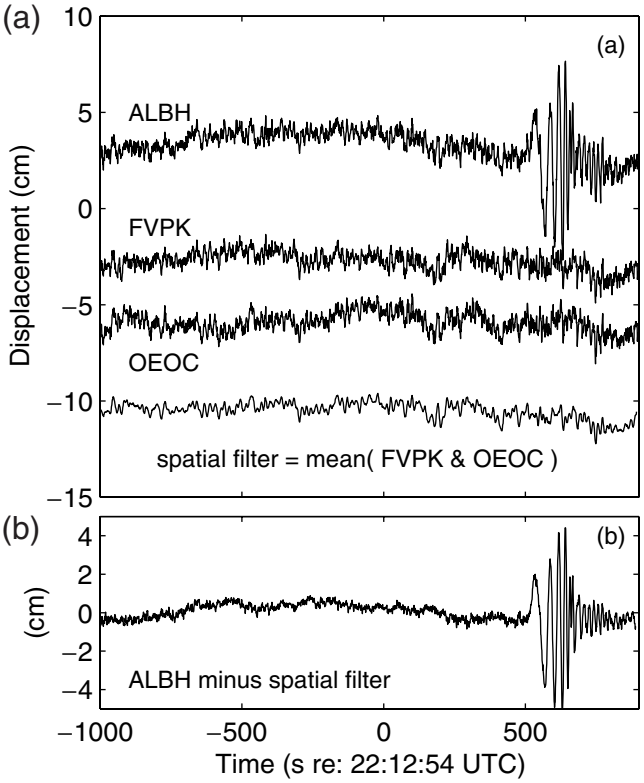

Figure 4. Spatial filtering of the east component at station ALBH. (a) To build the spatial filter, same-day positions of distant stations (OEOC and FVPK, over 1600 km distant from ALBH) after MSF are pointwise averaged and smoothed with a seven-point sliding boxcar. (b) To apply the spatial filter, the filter profile is subtracted from ALBH after MSF (Fig. 3), resulting in the final GPS seismogram.

filtering in the east component, with little net noise reduction in the north and vertical.

For the GPS data set described here, MSF and spatial filtering result in no significant change to the white noise part of the spectrum (Table 2); the 0.1–0.5-Hz band is dominated by random errors and the inherent noise floor of the specific receiver and station location. Station DSLK is an exception, with 0.05-cm reductions in white noise amplitude for the east and north components. DSLK is one of the noisiest sites in our network; MSF and spatial filtering bring the E and N noise floors into better agreement with the other Trimble 4000SSI receivers; for this particular station, what was previously assumed to be purely noise at 2–10-sec periods actually has a systematic component that is addressed by filtering, leaving only the random component.

For this network of GPS stations, what is the minimum amplitude of seismic waves observable by GPS? To answer this question, we quantify the absolute noise floor of our final (MSF and spatial filtered) GPS displacements by the rms error of the 1600 sec immediately before the Denali fault event began. The rms incorporates both the white noise and power law noise parts of the GPS error spectrum and therefore is a useful quantity for determining the detection threshold for seismic waves. For the stations analyzed here, the rms varies over ~0.4–1.0 cm for the horizontal components and 1.0–2.0 cm for the vertical (Table 2). These results are consistent with results from similar studies using a network analysis approach (e.g., Miyazaki *et al.*, 2004; Elósegui *et al.*, 2006) but slightly larger than instantaneous positioning over short baselines (e.g., Genrich and Bock, 2006). For the 2002 Denali event and this network, the noise floor of GPS prohibits detection of body waves; for example, *P* and *S* waves observed in British Columbia would have amplitudes of millimeters with energy at 1–10-sec periods. However, surface waves from this event had amplitudes of centimeters at 20–50-sec and longer periods and are therefore measurable by GPS. In the following sections, we describe broadband seismic recordings of the 2002 Denali event as observed in British Columbia and compare these surface-wave recordings to the GPS-derived surface-wave record of this event.

Seismic Data and Processing

In this article we analyze broadband seismic data from four stations of the CNSN that are effectively colocated with

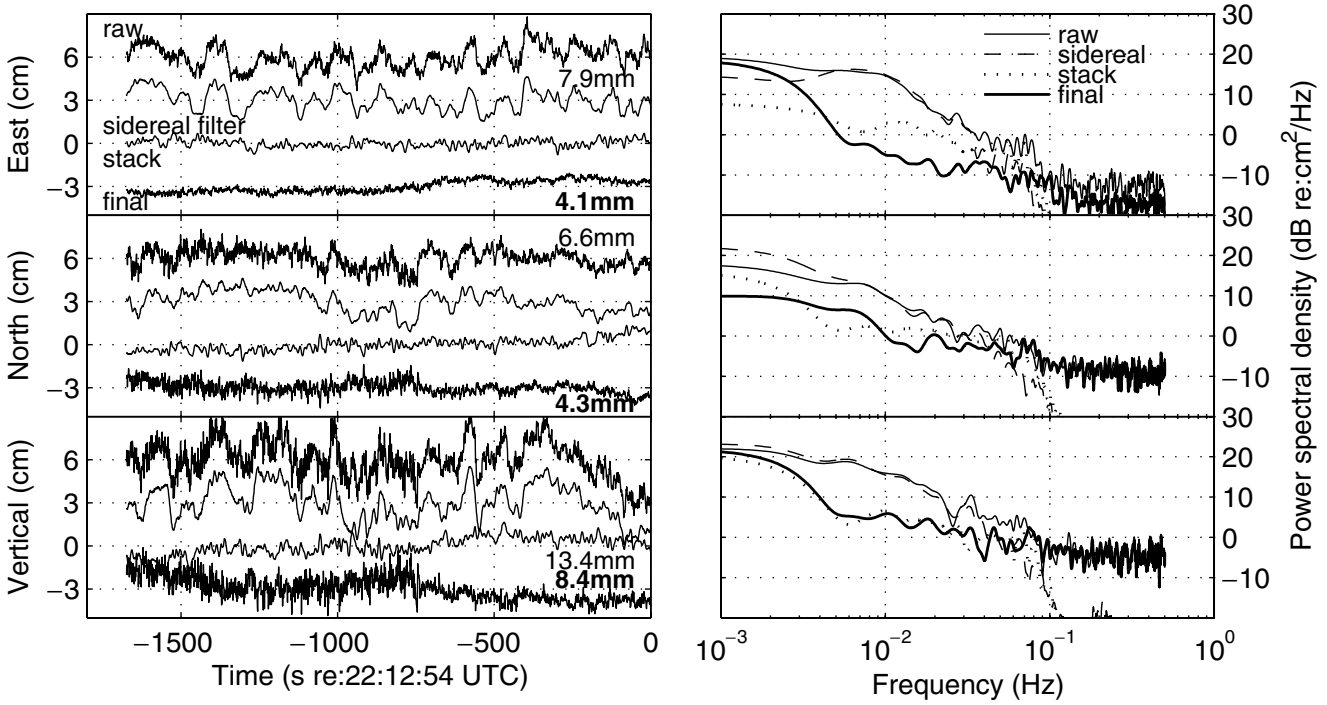

Figure 5. Positions and filtering stages for all three components of displacement at station ALBH for the ~1600 sec before the Denali fault event. The left-hand column provides GPS-derived time series: the raw time series (top trace), the MSF for ALBH (second trace), the spatial filter or stack for the subnetwork containing ALBH (third trace), and the final, filtered positions at ALBH (bottom trace). The rms of ALBH displacements before and after filtering are provided for each component. The right-hand column provides mean PSDs (i.e., PSDs for eight data segments with 50% overlap between adjacent segments are averaged together) for each series on the left.

continuous GPS stations (Table 4). The four seismic stations, at epicentral distances of 1093–2297 km, are DLBC, PNT, PGC, and PHC. These stations are colocated with the GPS sites DSLK, DRA2, PGC4, and PTHY, respectively (see Figure 1). Each of these seismic stations has a Guralp CMG 3ESP seismometer and GD Mark2 Digitizer operating at a sample rate of 40 Hz. These seismographs have a response that is flat in velocity from 30 sec to 50 Hz.

At these four sites, only the vertical component remained onscale (Cassidy and Rogers, 2004). The seismic data were processed as follows: remove any mean offset and trend; apply a cosine taper to the ends of the data window (5% of the signal length); remove instrument response; integrate to obtain displacement waveforms; and apply a 200-sec high-pass filter to remove very long-period noise. The resulting ground displacement waveforms (with amplitude given in centimeters) are shown in Figure 6. At all sites, the peak vertical ground displacement was between ±2–3 cm at a frequency of 0.0455–0.0588 Hz (period of 17–22 sec). A sample amplitude spectrum of the seismic ground displacement for station PGC is shown in Figure 7.

Table 4
Locations and Interstation Distances of Collocated Instruments

Site	Instrument Type	Distance (km)	Latitude (deg)	Longitude (deg)
DSLK	GPS	2.2	58.4358	230.0110
DLBC	BB		58.4372	229.9728
DRA2	GPS	< 1.0	49.3226	240.3750
PNT	BB		49.3160	240.3840
PGC4	GPS	< 1.0	48.6485	236.5490
PGC	BB		48.6500	236.5495
PTHY	GPS	4.6	50.6856	232.6247
PHC	BB		50.7067	232.5683

GPS receiver, GPS; broadband seismometer, BB.

Comparison of Broadband Seismic and GPS Data

In this section the vertical broadband seismic data are compared with the GPS data at the four sites with colocated instruments. The four site combinations (and interstation distances) are DLBC/DSLK (2.2 km), PHC/PTHY (4.6 km), PGC/PGC4 (< 1.0 km), and PNT/DRA2 (< 1.0 km). Because of the large horizontal ground velocities resulting from the Denali event, only the vertical component of each seismometer remained unclipped. We therefore begin by comparing unclipped seismometer and GPS displacement waveforms.

In Figure 8, the vertical component seismic and GPS data are compared. These represent the most precise (unclipped) seismic data but the least precise component of GPS data; as noted previously, the noise floor of GPS vertical positions is 2–3 times larger than noise in the horizontal components and has greater spectral power over all frequencies (Fig. 2, Tables 2 and 3). Even with the noise limitations of GPS, the

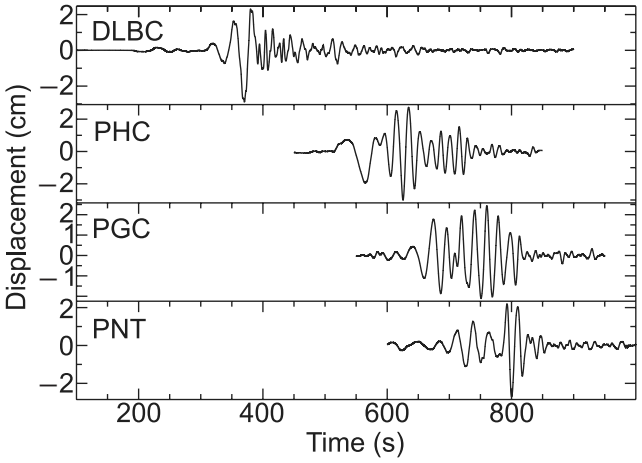

Figure 6. Vertical component ground displacement (cm) of the 2002 Denali earthquake plotted as a function of time (sec) for the four three-component broadband seismic stations of the CNSN discussed in text.

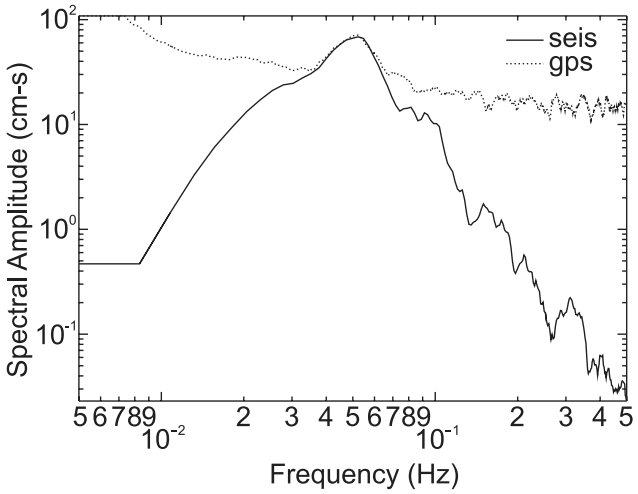

Figure 7. Amplitude spectrum for the vertical component of ground displacement at seismic station PGC (solid line) and GPS station PGC4 (dashed line). Most of the energy occurs in the frequency range of 0.03 Hz–0.07 Hz (or 14–30-sec period), which is typical of teleseismic events. Note the excellent agreement in this passband between the seismic and GPS spectra.

correspondence between the final GPS displacements and the integrated seismic waveforms is striking but difficult to clearly distinguish given the equivalent amplitude of GPS errors at several key frequencies of oscillation. In Figure 8, we also compare seismic and GPS waveforms that have been band-pass filtered from 10–50-sec period (0.02–0.1 Hz) as this passband contains most of the vertical surface wave energy (Fig. 7). After band-pass filtering, the waveforms match very well for amplitudes exceeding about 1-cm displacement. The agreement is nearly perfect for the largest amplitudes of the surface wave train at the stations PGC and PNT (Fig. 9). Note the nearly identical spectral match (Fig. 7) at frequencies from 0.035–0.065 Hz (15–29-sec period).

For this event and network of stations, the most precise GPS data coincides with the least precise seismic data (horizontal, but clipped). We demonstrate this by comparing all three components of displacement for sites PGC/PGC4 on Southern Vancouver Island (Fig. 1) at an epicentral distance of 2200 km. In Figure 10, we display seismic (solid) and GPS (dotted) waveforms without band-pass filtering. As described previously, the vertical component seismic waveform is unclipped and shows good agreement with the vertical component GPS waveform for the surface wave train, even given the similar noise and signal amplitudes in the GPS vertical. The larger amplitude north–south seismic component (±3–4 cm) was slightly clipped at PGC, with only 1 peak demonstrating minor clipping. The processed seismic waveform shows excellent agreement with the GPS signal; the latter has significantly less noise than the vertical. The largest amplitude surface waves (east–west component) are seriously clipped on the seismograph with eight severely clipped peaks. Processing this waveform as described earlier shows poor agreement with the GPS recording (as one might expect for a seriously clipped seismic record). Although the east–west seismic component is not useful, the GPS waveform captures the full range of displacement amplitudes (±6 cm) and, due to the combination of reduced noise floor and increased signal amplitude, accurately represents the surface waves.

Denali GPS Surface-Wave Data Set

For the 2002 Denali event, traditional seismometer recordings from instruments in northwestern North America were unable to capture the full magnitude of surface-wave displacements, as broadband seismometers in this region clipped, and no strong-motion seismometers were triggered (Cassidy and Rogers, 2004). However, the 23-station GPS network (Fig. 1) assembled for this study fills in the gaps in the surface wave seismic record of this event.

Figure 11 depicts a record section for all GPS stations in our network; only the east component is provided, as this was the most severely clipped component for the broadband seismometers. We show the waveforms after MSF and spatial filters were implemented as described previously, with the effect of reducing noise at surface wave frequencies (10–50-sec periods) without adversely affecting the character of the surface waves themselves. All three components (east–west, north–south, and vertical) of the final GPS seismograms for the 2002 Denali event are archived by IRIS as part of their permanent collection of seismic data, a first for geodetically determined displacements. These data products are now freely available to the scientific community at large under network code GD (geodetic displacements; www.iris.edu/mda/GD, last accessed February 2008) and may now be incorporated into studies of the event rupture history or crustal studies. These GPS data have previously been used

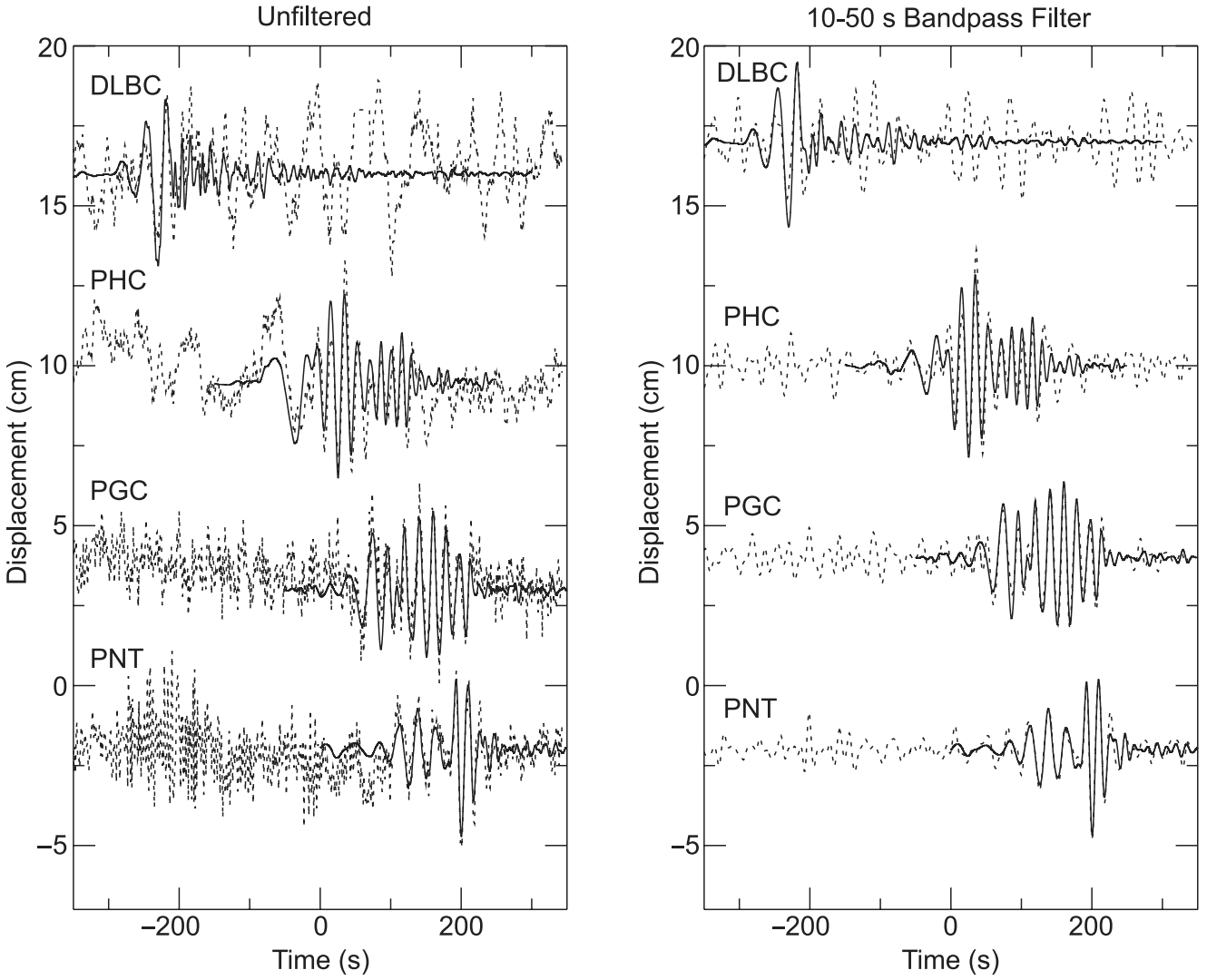

Figure 8. A comparison of the vertical component ground displacement (cm) of the 2002 Denali earthquake plotted as a function of time (in sec) for the four colocated seismic and GPS sites described in the text and Table 4. Solid lines denote seismic data integrated to displacement; dotted lines denote the GPS data. Both unfiltered (left) and band-pass filtered (10–50-sec period) waveforms are provided.

to study seismicity triggered by the Denali event (Gomberg *et al.*, 2004).

These 1-Hz GPS displacements properly capture surface waves propagating to the southeast from the Denali event and demonstrate several features of interest. For example, FAIR (~160 km from the epicenter) was the only station in our network with a measurable coseismic offset. Five stations (TEM1/TNK1/HNSC/FS32/ELDD) were present in the Skagway, Alaska, area at the time of the earthquake at 784–824-km epicentral distances; these stations display very similar waveforms but with an appropriate time lag with increasing distance. For stations at equivalent epicentral distances but different azimuths (e.g. PRDS and BREW at 2399 km), the surface wave characters differ significantly. Overall, the waveforms show appropriate dispersion and amplitude reduction with increasing distance.

Conclusions

In this study of the 2002 Denali earthquake, significant displacements were observed on GPS receivers at thousands of kilometers distance from the rupture. This was due to the nature of the Denali source mechanism (upper-crustal strike slip) and the optimal receiver location (along the rupture direction). Receivers placed at similar distances but perpendicular to the fault would have yielded much less impressive GPS seismograms. The 23 separate GPS recordings of this event provide important surface-wave records where seismometers either clipped or were simply not present. This study, along with studies of the 2003 Tokachi-Oki (Miyazaki *et al.*, 2004; Emore *et al.*, 2007) and 2003 San Simeon (Ji *et al.*, 2004; Wang *et al.*, 2007) events, demonstrates that high-rate GPS accurately measures large-amplitude motions

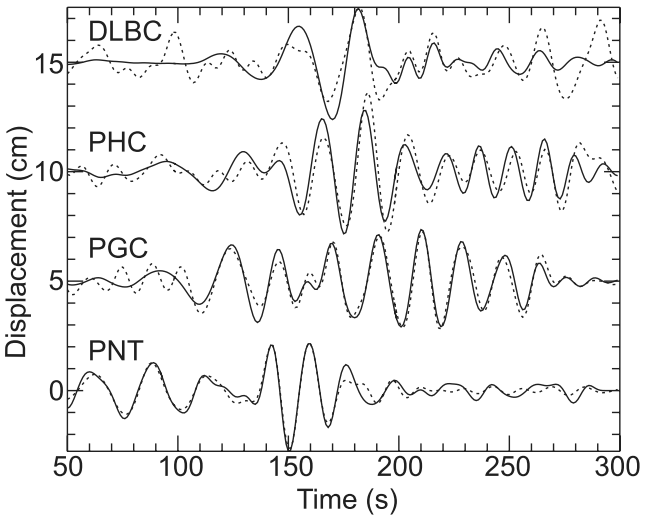

Figure 9. Close-up view of the 10–50-sec filtered vertical component surface waves from Figure 8. Solid lines denote seismic data integrated to displacement; dotted lines denote the GPS data.

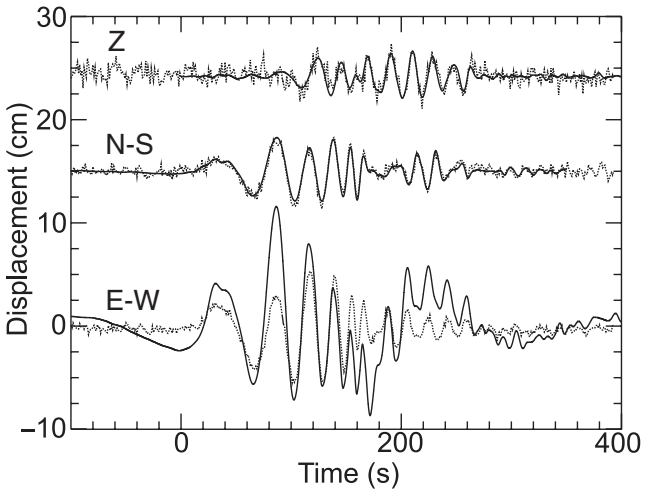

Figure 10. A comparison of all three components of ground displacement (cm) of the 2002 Denali earthquake plotted as a function of time (sec) for the collocated instruments PGC/PGC4 on southern Vancouver Island. Solid lines denote seismic data integrated to displacement; dotted lines denote the GPS data. Note that for the seismic data, the vertical component waveform is most precise (unclipped), whereas the north–south component is slightly clipped (1 peak), and the east–west component is least accurate (eight peaks in the surface-wave train are significantly clipped). For the GPS data, the opposite is true: the large-amplitude horizontal component data are most precise, and the vertical component is least precise.

during earthquakes. The value of high-rate GPS to earthquake studies will ultimately depend on how close receivers are to the rupture and whether they can augment existing seismic instrumentation. While dynamic displacements for smaller-magnitude earthquakes may not be observable by high-rate GPS, the error-reduction techniques described in this article can be used to determine a more accurate measurement of the static offset, especially for earthquakes with significant afterslip (e.g., the Parkfield event [Langbein *et al.*, 2005]).

The GPS results presented here are unique in both the continental scale of the network and the mix of receiver types; most other high-rate GPS earthquake studies have involved networks much closer to the epicenter with smaller interstation distances. With this mixed receiver network spread over 45°–65° latitudes at 150–3000-km epicentral distances using four different classes of geodetic dual-frequency GPS receivers, noise characteristics of the displacement time series were analyzed. We note that the lower limit of noise in high-rate GPS positions is a complicated combination of station latitude, satellite geometry, MSF, and spatial filter implementation, as well as individual receiver model. We discussed the impact of sidereal and spatial filtering on the position time series through changes in white noise amplitude and power law behavior. The absolute noise floor of GPS positions (as determined by rms) is ~0.4–1.0 cm for the horizontal components and 1.0–2.0 cm for the vertical, and after error-reduction stages, the GPS positions are described largely as flicker noise.

In addition, we compared integrated broadband seismometer records (clipped and unclipped) and collocated GPS displacements to both validate the GPS recordings and demonstrate the relative strengths of each instrument type. For amplitudes exceeding about 1.0-cm displacement, the 1-Hz GPS and unclipped seismic waveforms are in good agreement for the surface wave train from the Denali earthquake. Where seismic data are clipped (horizontal components), GPS data accurately measures the ground motion; where GPS data are not as well resolved due to small amplitudes and a larger noise floor (e.g., vertical component data), the seismic data more accurately measure the ground motions. Combining these two data sets to account for their relative strengths (e.g., Wang *et al.*, 2007) may lead to more accurate modeling and imaging of earthquake rupture sequence and source parameters.

Overall, GPS positioning has many advantages for seismologic applications, namely, direct determination of displacement without integration and the ability to remain onscale during large events with significant displacements. Seismometers have nearly the opposite behavior, requiring integration of velocity or acceleration to recover displacement and potentially clipping or saturating under the extreme accelerations associated with very large earthquakes. High-rate GPS still has some limitations for seismologic applications, however. Primarily, the noise floor of high-rate GPS dictates that displacements must be half a centimeter or more in order to be detectable by GPS. Also, GPS displacements are estimates resulting from the least-squares process and not direct measurements (unlike the velocity and acceleration measurements from seismometers), and consequently residual error sources propagate into the displacements. These residual errors are largely addressed through modified sidereal and spatial filtering, allowing a larger range of seismic waves (amplitude and frequency) to be detectable and resolvable with GPS.

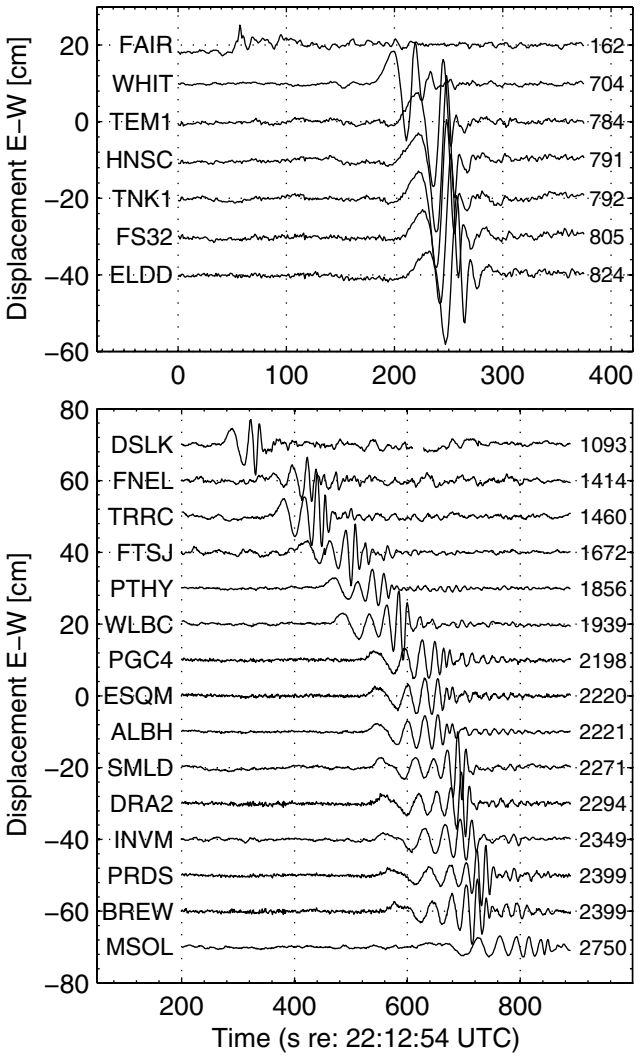

Figure 11. Plot of the east component of displacement for 22 GPS stations of interest (Fig. 1), with stations offset for clarity and the epicentral distance (km) provided on the right-hand side. Note the change in *x*-axis length between the top and bottom plots. Station YELL was omitted, as its location is largely off axis of the line of preferential directivity.

Acknowledgments

We thank Garry Rogers for helpful discussions and are indebted to Herb Dragert and Jeff Freymueller for making a substantial portion of these high-rate GPS data available. We also thank Rick Benson at IRIS for archiving the GPS data for public use. Comments from two anonymous reviewers improved the manuscript. Continuously operating GPS infrastructure support is provided by NRCan for stations in Canada, and by IGS, the National Geodetic Survey (NGS), UNAVCO, the Jet Propulsion Laboratory (JPL), the Southern California Integrated GPS Network (SCIGN), the U.S. Geological Survey (USGS), the Keck Foundation, and the National Aeronautics and Space Administration (NASA) for stations in the United States; campaign GPS data from the Skagway area were provided by AeroMap USA. Seismic waveforms used in this study are from the Canadian National Seismic Network, operated by the Geological Survey of Canada. The authors gratefully acknowledge support from a USGS grant to assess high-rate GPS as a strong-motion sensor (Grant Number 05HQGR0015), National Science Foundation (NSF) grants on high-rate GPS (Grant Number EAR-0337206) and multipath (Grant Number EAR-0003943), an NSF graduate student research fellowship (AB), and a University of Colorado Faculty Fellowship (KL). Geological Survey of Canada/Earth Science Sector Contribution Number 20070150.

References

Agnew, D. C. (1992). The time-domain behavior of power-law noise, *Geophys. Res. Lett.* **19,** 333–336.

Aki, K., and P. G. Richards (1980). *Quantitative Seismology: Theory and Methods*, W. H. Freeman, New York

Altamimi, Z., P. Sillard, and C. Boucher (2002). ITRF2000. new release of the international terrestrial reference frame for earth science applications, *J. Geophys. Res.* **107,** no. B10, doi 10.1029/2001JB000561.

Beutler, G., M. Rothacher, S. Schaer, T. A. Springer, J. Kouba, and R. E. Neilan (1999). The International GPS Service (IGS): an interdisciplinary service in support of earth sciences, *Adv. Space Res.* **23,** no. 4, 631–635, doi 10.1016/S0273-1177(99)00160-X.

Bilich, A. L. (2006). Improving the precision and accuracy of geodetic GPS: applications to multipath and seismology, *Ph.D. Thesis*, University of Colorado.

Bock, Y., L. Prawirodirdjo, and T. I. Melbourne (2004). Detection of arbitrarily dynamic ground motions with dense high-rate GPS network, *Geophys. Res. Lett.* **31,** doi 10.1029/2003GL019150.

Boore, D. M., C. D. Stephens, and W. B. Joyner (2002). Comments on baseline correction of digital strong-motion data: examples from the 1999 Hector Mine, California earthquake, *Bull. Seismol. Soc. Am.* **92,** no. 4, 1543–1560, doi 10.1785/0120000926.

Cassidy, J. F., and G. C. Rogers (2004). The M_w 7.9 Denali fault earthquake of 3 November 2002: felt reports and unusual effects across western Canada, *Bull. Seismol. Soc. Am.* **94,** S53–S57, doi 10.1785/0120040607.

Choi, K., A. Bilich, K. M. Larson, and P. Axelrad (2004). Modified sidereal filtering: implications for high-rate GPS positioning, *Geophys. Res. Lett.* **31,** no. 22, L22608, doi 10.1029/2004GL021621.

Eberhart-Phillips, D., P. J. Haeussler, J. T. Freymueller, A. D. Frankel, C. M. Rubin, P. Craw, N. A. Ratchkovski, G. Anderson, G. A. Carver, A. J. Crone, T. E. Dawson, H. Fletcher, R. Hansen, E. L. Harp, R. A. Harris, D. P. Hill, S. Hreinsdottir, R. W. Jibson, and L. M. Jones (2003). The 2002 Denali fault earthquake, Alaska: large magnitude, slip-partitioned event, *Science* **300,** no. 5622, 1113–1118, doi 10.1126/science.1082703.

Elósegui, P., J. L. Davis, D. Oberlander, R. Baena, and G. Ekstrôm (2006). Accuracy of high-rate GPS for seismology, *Geophys. Res. Lett.* **33,** L11308, doi 10.1029/2006GL026065.

Emore, G., J. Haase, K. Choi, K. M. Larson, and A. Yamagiwa (2007). Recovering absolute seismic displacements through combined use of 1-Hz GPS and strong motion accelerometers, *Bull. Seismol. Soc. Am.* **97,** 357–378.

Ge, L., S. Han, C. Rizos, Y. Ishikawa, M. Hoshiba, Y. Yoshida, M. Izawa, N. Hashimoto, and S. Himon (2000). GPS Seismometers with up to 20 Hz sampling rate, *Earth Planets Space* **52,** 881–884.

Genrich, J. F., and Y. Bock (1992). Rapid resolution of crustal motion at short ranges with the Global Positioning System, *J. Geophys. Res.* **97**, no. B3, 3261–3269, doi 10.1029/91JB02997.

Genrich, J. F., and Y. Bock (2006). Instantaneous geodetic positioning with 10–50 Hz GPS measurements: noise characteristics and implications for monitoring networks, *J. Geophys. Res.* **111,** B03403, doi 10.1029/2005JB003617.

Global Centroid Moment Tensor (CMT) Project catalog search, www.globalcmt.org/CMTsearch.html (last accessed February 2008).

Gomberg, J., P. Bodin, K. Larson, and H. Dragert (2004). Earthquake nucleation by transient deformations caused by the M = 7.9 Denali, Alaska, earthquake, *Nature* **427,** 621–624, doi 10.1038/nature02335.

Ji, C., K. M. Larson, Y. Tan, K. W. Hudnut, and K. Choi (2004). Slip history of the 2003 San Simeon earthquake constrained by combining 1-Hz GPS, strong motion, and teleseismic data, *Geophys. Res. Lett.* **31,** no. 17, L17608, doi 10.1029/2004GL020448.

Kouba, J. (2003). Measuring seismic waves induced by large earthquakes with GPS, *Stud. Geophys. Geod.* **47,** 741–755.

Langbein, J., R. Borcherdt, D. Dreger, J. Fletcher, J. L. Hardebeck, M. Hellweg, C. Ji, M. Johnston, J. R. Murray, R. Nadeau, M. J. Rymer, and J. A. Treiman (2005). Preliminary report on the 28 September 2004. 6.0 Parkfield, California earthquake, *Seism. Res. Lett.* **76,** 10–26.

Larson, K. M., A. Bilich, and P. Axelrad (2007). Improving the precision of high-rate GPS, *J. Geophys. Res.* **112,** B05422, doi 10.1029/2006JB004367.

Larson, K., P. Bodin, and J. Gomberg (2003). Using 1-hz GPS data to measure deformations caused by the Denali fault earthquake, *Science* **300,** 1421–1424, doi 10.1126/science.1084531.

Lichten, S., and J. Border (1987). Strategies for high-precision Global Positioning System orbit determination, *J. Geophys. Res.* **92,** 12,751–12,762.

Miyazaki, S., K. M. Larson, K. H. Choi, K. Hikima, K. Koketsu, P. Bodin, J. Haase, G. Emore, and A. Yamagiwa (2004). Modeling the rupture process of the 2003 September 25 Tokachi-Oki (Hokkaido) earthquake using 1-Hz GPS data, *Geophys. Res. Lett.* **31,** L21603, doi 10.1029/2004GL021457.

Ohta, Y., I. Meiano, T. Sagiya, F. Kimata, and K. Hirahara (2006). Large surface wave of the 2004 Sumatra-Andaman earthquake captured by the very long baseline kinematic analysis of 1-Hz GPS data, *Earth Planets Space* **58,** 153–157.

Ozacar, A. A., S. L. Beck, and D. H. Christensen (2003). Source process of the. November 2002 Denali fault earthquake (central Alaska) from teleseismic observations, *Geophys. Res. Lett.* **30,** 1638, doi 10.1029/2003GL017272.

Parkinson, B. W., J. J. Spilker Jr., P. Axelrad and P. Enge (Editors) (1996). *Global Positioning System: Theory and Applications*, Am. Inst. Aeronaut. Astron., Reston, Virginia.

Segall, P., and J. L. Davis (1997). GPS Applications for Geodynamics and Earthquake Studies, *Ann. Rev. Earth Planet. Sci.* **25,** 301–336.

Velasco, A. A., C. J. Ammon, J. Farrell, and K. Pankow (2004). Rupture directivity of the November 2002 Denali fault earthquake determined from surface waves, *Bull. Seismol. Soc. Am.* **94,** no. 6B, S293–S299, doi 10.1785/0120040624.

Wang, G., D. M. Boore, G. Tang, and X. Zhou (2007). Comparisons of ground motions from collocated and closely spaced one-sample-per-second Global Positioning System and accelerograph recordings of the 2003 M 6.5 San Simeon, California, earthquake in the Parkfield Region, *Bull. Seismol. Soc. Am.* **97,** no. 1B, 76–90, doi 10.1785/0120060053.

Wdowinski, S., Y. Bock, J. Zhang, P. Fang, and J. Genrich (1997). Southern California permanent GPS geodetic array: spatial filtering of daily positions for estimating coseismic and postseismic displacements induced by the 1992 Landers earthquake, *J. Geophys. Res.* **102,** 18,057–18,070.

National Geodetic Survey
325 Broadway E/GC2
Boulder, Colorado 80305
Andria.Bilich@noaa.gov
(A.B.)

Natural Resources Canada
Geological Survey of Canada
9860 W. Saanich Rd.
Sidney, BC V8L 4B2 Canada
cassidy@pgc.nrcan.gc.ca
(J.F.C.)

Department of Aerospace Engineering Sciences
University of Colorado
UCB 429
Boulder, Colorado 80309-0429
kristinem.larson@gmail.com
(K.M.L.)

Manuscript received 16 April 2007